2008 IEEE International Conference on
Robotics and Automation
Pasadena, CA, USA, May 19-23, 2008

Modeling and Analysis of DNA Hybridization Dynamics at Microarray Surface in Moving Fluid

Tad Hogg Mingjun Zhang Ruoting Yang

Abstract— **This paper proposes a dynamic model of DNA microarray hybridization properties in moving fluid. Prior experimental studies indicate hybridization efficiency is closely related to fluid dynamics, temperature, DNA probe density and microarray surface properties. Simulation results using the model proposed here agree well with practical observations. The model may be used to improve and manipulate performance of DNA microarray hybridization, and implement as a control model for hybridization automation to improve reliability and robustness of microarray hybridization process.**

I. INTRODUCTION

DNA microarrays are a dominant platform for genomics research. More recently, these arrays have been applied to medical diagnostics [1], [2].

One challenge for DNA microarray applications is obtaining reliable microarray signals, which are often affected by hybridization dynamics including fluid velocity, temperature, and surface properties. For example, one surface property, the density of binding sites, affects the binding reaction rate. In addition, surface flatness also determines orientations of single-stranded DNAs attached to the surface and affect the DNA binding signal. Hybridization dynamics, especially in fluid, often cannot be well controlled, which results in false negative signals. Moreover, the time required to obtain results is often determined from trial and error. Effective control over the hybridization process could automate system adjustments to give reliable microarray signals. An automated hybridization process can also improve robustness of the process and provide high throughput. Most current microarray hybridization techniques are passive hybridization that may take several hours [3]. Some automated systems and new methods have been proposed to increase the hybridization efficiency, including DIG Easy Hyb system from Roche and using the photovoltaic effect [4]. Unfortunately, no highly accurate dynamic model is used for these systems. The system parameter setup is mainly based on experiences. This has been an obstacle to obtain reliable and repeatable microarray signals.

The microrray signal depends on the hybridization efficiency with which available DNA strands in the fluid hybridize with the binding sites. The hybridization efficiency is determined by multiple dynamic and kinetic factors of the process, including fluid velocity, temperature, and the probe density. Unfortunately, measuring how these variables affect DNA binding at the molecular level is difficult. One reason for this difficulty is hybridization behaviors are not simply related to conventional binding rates seen in biochemistry that is usually in solution. Instead, hybridization also depends significantly on the environment of the binding site. For example, hybridization depends strongly on probe density in both the efficiency of duplex formation and the kinetics of target capture [5]. As discussed in [6] and [7], both temperature and fluid flow have important effects to the hybridization results. Knowing precisely how these factors affect microarray hybridization is critical to improve and manipulate microarray performance.

Hybridization process automation, including microfluidics, temperature and hybridization time control, can make the hybridization more robust and parallel with high throughput. An important issue for hybridization automation is developing a mathematical model to capture the key factors affecting hybridization results such as diffusion, fluid dynamics, temperature and timing effects. These factors can affect hybridization performance in two ways. First, at a system level, they alter the rate at which target molecules in the fluid reach the binding spots on the microarray array. Second, at a microscopic level, they affect the efficiency (i.e., rate) of single strand binding. These effects can compete against each other, leading to tradeoffs in the design of the array and its operating environment. Further study of these effects is necessary due to the concerns that 1) quantitative measures of target capture during DNA microarray hybridization remain an open issue; 2) consequences of multiple physical effects on hybridization has not been well discussed in the literature; and 3) improved understanding may provide quantitative guidance to regulate the hybridization process. Though automated hybridization systems exist (such as DIG Easy Hyb) in the market, no quantitative model for hybridization automation has been proposed in the open literature. Thus while existing systems provide a solution, other approaches may lead to more effective hybridization, e.g., using control based on a precise dynamic model of hybridization. Control based on such models should be more effective and robust than using trial and error to establish parameters.

Some dynamics modeling of the DNA hybridization process has been reported. For example, models show how temperature and the presence of mismatched binding affects the signal [8], but without the effects of fluid flow. Kim, et al. [9] reported the influence of flow rate, velocity, DNA concentration, height of the channel and time on

T. Hogg is at Hewlett-Packard Laboratories, Palo Alto, CA, USA tad.hogg@hp.com

M. Zhang is at Department of Mechanical, Aerospace and Biomedical Engineering, University of Tennessee, Knoxville, TN, USA mjzhang@utk.edu

R. Yang is at Department of Electrical and Systems Engineering, Washington University, St. Louis, MO, USA ruoting@ese.wustl.edu

978-1-4244-1647-9/08/$25.00 ©2008 IEEE.

DNA hybridization kinetics. Numerical models also allow investigating fluid transport effects [7]. The application for these models, and that discussed in this paper, is for closed microfluidic flow channels, which creates a laminar fluid flow between two parallel plates whose width is much larger than the spacing between the plates. Modeling DNA binding dynamics at microarray surfaces in fluid is an open issue, particularly finding appropriate tradeoffs between accuracy of physical effects and knowledge of the necessary model parameters to allow effective automation. This paper presents a differential-equation based model of array performance and uses the model to determine how array performance depends on fluid velocity, temperature and probe density. Simulation results are presented to validate the model against practical observations. This paper is organized as follows. Sec. II describes the model. Sec. III discusses simulation results and analysis. Hybridization automation is proposed in Sec. IV. The paper ends with discussions and conclusions in Sec. V.

II. MODEL DESCRIPTION

DNA microarray hybridization usually occurs in a hybridization chamber, as indicated schematically in Fig. 1. The hybridization chamber consists of two flat plates, spaced a distance H apart, and with length and width of 2 and 4 inches, respectively. The microarray is centered on the bottom layer, containing tens of thousands of DNA spots. A whole human genome can be printed in a single chip. Recent chips can contain DNA probes ranging from 10^3-10^6 spots. Each spot is usually for a distinct DNA molecule, and includes about 10^8 single stranded DNA molecules for binding complementary DNA molecules in the fluid passing over the microarray. This number is obtained by assuming a spot size of 50 micron in diameter and each strand occupies an area 4×4 nanometer square area. The single-strand molecules in a binding site are all the same.

When complementary DNA molecules encounter the single-stranded DNA in a spot, they bind to available unbound molecules on the surface. The result of the process is detected optically by fluorescence signal.

For simplicity, this paper focuses on the behavior of a single binding site, with diameter L. We thus only consider concentration of its associated DNA in the fluid. To focus on fluid effects, we treat each binding site independently, i.e., ignore any binding of mismatched DNA since it occurs at a much lower rate. This assumption means we do not model false positives, though that would be a simple extension of our model by considering another component in the fluid: a mismatched DNA with lower affinity for the binding strands than the true signal (an exact complementary match) [8].

We consider a two-dimensional slice through the container, passing through the center of one of the binding sites, as shown in Fig. 1. This approximation ignores effects of the finite width of the binding site. We take the fluid to flow in positive x direction and channel extending from the bottom plane at $y = 0$, with the binding site, to $y = H$ for the upper plate. We consider a segment of the length of the channel of length $X_0 > L$. Specifically we take the upstream end

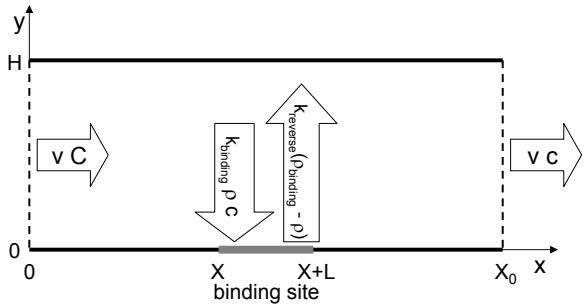

Fig. 1. Schematic of slice through container. The binding site, of diameter L, is shown in gray along the lower boundary. Arrows indicate boundary conditions for the flux of the chemical dissolved in the fluid at the inlet (left), outlet (right), and binding site. Fluid flows from left to right through the channel.

of the segment to be at $x = 0$, the binding site to extend over $X \le x \le X + L$ and the downstream end of the channel segment at $x = X_0$. In this geometry, the fluid flow is simple so the main effect of fluid dynamics arises through the speed of the flow. Hence we focus on fluid velocity in our study. Nevertheless, our model applies to more complex geometries, e.g., channels with variable widths, which would involve more complex fluid motions.

A. Behavior in the Fluid

For the flow speeds relevant here, the Reynolds number is small and flow is laminar. For this geometry, with pressure-driven flow the fluid velocity profile is parabolic: the velocity (in the positive x direction) at location y is [10]

$$v = 6v_{\text{avg}} \frac{y(H-y)}{H^2} \tag{1}$$

for $0 \le y \le H$. The gradient in fluid velocity at the surface $y = 0$ is $6v_{\text{avg}}/H$ where v_{avg} is the average speed of the fluid in the channel.

The chemical of interest is dissolved in the fluid with concentration C. This fluid flows through the channel past the binding site. The chemical moves with the fluid and also diffuses through the fluid. The concentration function $c(x, y, t)$, giving the concentration of the chemical at location x, y in the channel at time t, satisfies the diffusion equation [11]

$$\frac{\partial c}{\partial t} + \nabla \cdot F = 0 \tag{2}$$

where $F = -D\nabla c + vc$ is the chemical flux, and v is the fluid velocity (in the x direction) given by Eq. (1).

We take the initial concentration in the fluid by the binding site to be zero, i.e., $c(x, y, 0) = 0$. This contrasts with the initial value $c(x, y, 0) = C$ used in other models [8] where the time required for significant reaction (minutes to hours) is much longer than the time for the initial fluid with the chemical to reach the array (seconds). We impose the boundary condition on the inlet boundary that $F = vC$ in the positive x direction corresponding to the chemical flowing into the channel segment with the fluid. We assume the outlet is far enough downstream of the binding site that

concentration gradients in the x direction are negligible, giving the boundary condition $F = vc$, again in the positive x direction for the flow out of the channel segment. The lower and upper surfaces of the channel do not allow fluid or chemical to pass, giving $F = 0$ in the direction normal to the surface (i.e., the y direction). The binding site, as part of the lower surface, is an exception: the flux normal to the surface at the binding site is $F = F_{\text{binding}}$, which is proportional to the concentration as described below. The positive value of this flux gives the net rate molecules leave the fluid by binding to the strands in the binding site. Fig. 1 summarizes these boundary conditions. The flux at the inlet is constant in time, while the fluxes at the outlet and binding site varies with time as the concentration c changes.

B. Behavior at Binding Site

Only single-stranded DNA's occupy the binding site initially. During the hybridization, the single-stranded DNAs bind with the matching DNA diffusing to them as the fluid moves over the site. Let $\rho(x,t)$ be the surface density of single-stranded DNAs at position x and time t. Initially, $\rho(x,0) = \rho_{\text{binding}}$ and

$$\frac{\partial \rho}{\partial t} = -F_{\text{binding}} \tag{3}$$

so the net flux of chemicals to the binding site gives the rate at which strands become occupied (i.e., once occupied, strands remain occupied) and hence the rate at which ρ decreases.

To evaluate F_{binding}, consider the reaction

$$\text{unbound strand} + \text{molecule} \rightarrow \text{bound strand}$$

which we take to occur at a rate proportional to concentration of the reactants, in this case the density of unbound strands (ρ) and concentration of chemical in the fluid at the binding site (c).

We define k_{binding} as the binding rate constant and k_{reverse} as the rate constant for the reverse reaction. The net reaction rate is then

$$F_{\text{binding}} = k_{\text{binding}} \rho c - k_{\text{reverse}} (\rho_{\text{binding}} - \rho) \tag{4}$$

C. Model Parameters

Table I gives the nominal parameter values for the model. Most of the parameter values are based on experimental estimates, and can vary somewhat depending on the application. For example, we consider a specific concentration C used in other studies [12], [13]. For parameter measurements in fluids, many sensor and experimental techniques have been developed specifically for DNA hybridization [14], [15].

The reaction rate parameters, k_{binding} and k_{reverse}, are not well-characterized empirically, and various authors propose a range of values in models of DNA arrays. In particular, the surface of the DNA array can alter reaction behavior compared to that seen for reactions in solutions.

For binding to single-stranded DNA, the binding reaction rate has only limited change over normal operating temperatures [8], and we consider k_{binding} to be independent of temperature. However, the binding rate depends on the surface density of binding sites. In particular, the binding involves two mechanisms: a relatively slow reaction from bulk solution to the probe, and a relatively fast reaction from target molecules adsorbed on the surface (and diffusing in two dimensions) [16]. When the binding site density is low, the overall rate is dominated by the faster process, giving $k_{\text{binding}} \approx 10^6/\text{M/s}$, but at higher binding site densities surface diffusion is reduced. At a sufficiently high density, which we denote as $\rho_{\max}$, the surface diffusion is blocked so only the slower process operates, with reaction rate around $10^5/\text{M/s}$. Instead of a detailed model of this process including surface diffusion explicitly [16], we consider a simplified model combining the surface and bulk processes to give

$$k_{\text{binding}} = 10^5/\text{M/s} + (1 - \rho_{\text{binding}}/\rho_{\max}) 10^6/\text{M/s} \tag{5}$$

with $0 < \rho_{\text{binding}} \leq \rho_{\max}$

The reverse reaction is strongly temperature dependent. We use the Arrhenius equation as a functional form for this dependence, i.e.,

$$k_{\text{reverse}} = A \exp(-B/T) \tag{6}$$

where T is the absolute temperature and A, B are positive constants.

To calibrate the parameters A, B, we use empirical observations of the change in equilibrium binding with temperature along with $k_{\text{binding}} \approx 10^6/\text{M/s}$ appropriate for low strand densities. The equilibrium density of unbound strands after exposure to a fixed concentration c for a long time occurs when $F_{\text{binding}} = 0$, giving an equilibrium fraction $f \equiv \rho/\rho_{\text{binding}}$ remaining unbound of

$$f = \frac{k_{\text{reverse}}}{k_{\text{binding}} c + k_{\text{reverse}}} \tag{7}$$

Furthermore, in a region with a fixed concentration c, Eq. (4) gives the relaxation to the equilibrium value as proportional to $\exp(-t/\tau)$ with the time scale

$$\tau = \frac{1}{k_{\text{binding}} c + k_{\text{reverse}}} \tag{8}$$

DNA hybridization is very sensitive to temperature over the range of 54 to 93 degrees C [17]. Specifically, at concentrations around 100 nanomolar, the arrays change from high equilibrium binding to essentially none as temperature changes from $T = 54°\text{C}$ to $93°\text{C}$. From these observations, we pick values for the parameters A,B in Eq. (6) so the equilibrium unbound fraction f changes from 5% at $54°\text{C}$ to 95% at $93°\text{C}$. Table I shows the resulting values.

In practice, the concentration c varies both in space and time, depending on the fluid flow and diffusion. Thus while Eq. (7) and (8) give rough estimates, evaluating the actual equilibrium binding and time scales requires a solving the full equations, including diffusion of Eq. (2).

TABLE I

PARAMETER VALUES USED IN THE MODEL SIMULATION. THE REVERSE REACTION PARAMETERS DETERMINE THE TEMPERATURE DEPENDENCE OF k_{reverse} VIA EQ. (6). THE TABLE GIVES RANGES FOR FLUID SPEED, STRAND DENSITY AND TEMPERATURE WE CONSIDER WITH SIMULATIONS, AND THE CORRESPONDING RANGES FOR k_{binding} (WHICH DEPENDS ON STRAND DENSITY) AND k_{reverse} (WHICH DEPENDS ON TEMPERATURE).

parameter	value
container	
container height	$H = 1.5\text{mm}$
binding site	
diameter	$L = 50\mu\text{m}$
number density of DNA strands	$\rho_{\text{binding}} = 5 \times 10^{14}$ to $5 \times 10^{16}/\text{m}^2$
maximum possible strand density	$\rho_{\max} = 6 \times 10^{16}/\text{m}^2 = 10^{-7}\text{mole}/\text{m}^2$
fluid	
average fluid velocity	$v_{\text{avg}} = 10^{-4}$ to $10^{-2}\text{m}/\text{s}$
fluid temperature	$T = 35$ to $90°\text{C}$
chemical	
concentration	$C = 6 \times 10^{19}\text{molecule}/\text{m}^3 = 0.1\mu\text{M}$
diffusion coefficient	$D = 10^{-10}\text{m}^2/\text{s}$
binding reaction rate	$k_{\text{binding}} = 10^5$ to $1.1 \times 10^6/\text{M}/\text{s}$
reverse reaction rate	$k_{\text{reverse}} = 1.7 \times 10^{-4}$ to $1.3/\text{s}$
reverse reaction parameters	$A = 5.4 \times 10^{21}/\text{s}$
	$B = 18087°\text{K}$

III. SIMULATIONS AND ANALYSIS

To evaluate hybridization array performance, we solved the model equations numerically using finite element techniques, dividing the fluid domain into 4652 grid elements with grid points constrained to be no more than a micron apart on the binding site to give detailed coverage of binding behavior.

To illustrate the qualitative behavior of the model, we consider a case with $\rho_{\text{binding}} = 5 \times 10^{16}/\text{m}^2$, $v_{\text{avg}} = 10^{-3}\text{m}/\text{s}$ and $T = 37°\text{C}$. Fig. 2 shows how the density of single-strand DNA changes on the binding site. Initially the density is $\rho(x, 0) = \rho_{\text{binding}}$ and decreases with time. The density decreases most rapidly at the upstream edge of the binding site (on the left side of the figure) where the fluid first reaches the binding site. The density at the downstream edge decreases more rapidly than at intermediate locations because binding sites at the downstream edge have less competition with other binding sites for the diffusing chemical than sites in the middle of the binding region.

In this example, the combination of fluid speed and chemical diffusion means most of the binding arises from the chemicals moving in the fluid near the surface, as illustrated in Fig. 3. This figure shows most of the incoming concentration passes the binding site without time for diffusion to bring the chemical to the site. Only fluid passing close to the bottom of the channel provides sufficient opportunity for diffusion.

The remainder of this section describes case studies that vary the model parameters to match different experimental conditions.

A. Fluid velocity versus hybridization efficiency

From Fig. 4, we can see that the time to reach 90% equilibrium binding decreases as the average fluid speed is increased. This means the DNA hybridization efficiency increases as the fluid velocity increases. The conclusion is consistent with practical observations [13], [16]. In addition, the hybridization efficiency saturates at large velocities.

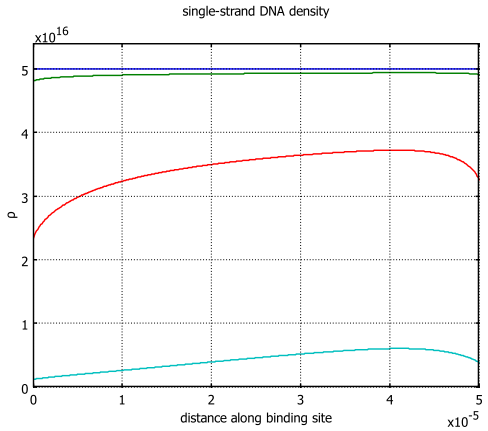

Fig. 2. Density of single-strand DNA, ρ, on the binding site. The horizontal axis is distance along the binding site, in units of 10^{-5} meters. The densities on the vertical axis are in units of $10^{16}/\text{m}^2$. The top line is the initial density, $\rho = \rho_{\text{binding}}$. The remaining curves show the density after 5, 50 and 200 seconds, from top to bottom, respectively.

B. DNA site density versus hybridization efficiency

Fig. 5 shows the effects of binding site density. At low temperatures, the reverse reaction rate is so low that even the slow binding process is sufficient to produce full equilibrium binding even if the binding site density is high. So equilibrium binding is linear in the binding site density.

C. Temperature versus hybridization efficiency

As shown in Fig. 6, the number of bound strands in equilibrium decreases as the temperature increases. The rate varies with binding site densities, with more rapid decrease at higher binding site densities. From an automation perspective, this behavior means different hybridization temperatures

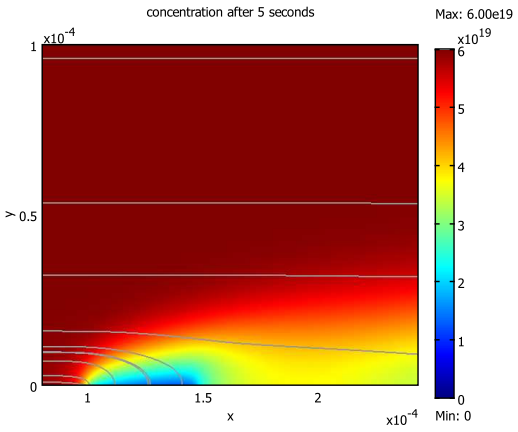

Fig. 3. Concentration $c(x, y, t)$ at time $t = 5$s. Distances along the axes are in units of 10^{-4} meters, and the concentration varies from 0 (dark blue) to $C = 6 \times 10^{19}$molecule/m^3 (red). The binding site is located along the bottom axis between tick marks 1 and 1.5. The curves across the plot are some streamlines of the chemical flux, showing most of the flux to the binding site arises from fluid moving within a few microns of the bottom of the channel (at $y = 0$). The figure shows only a small portion of the full channel width and length.

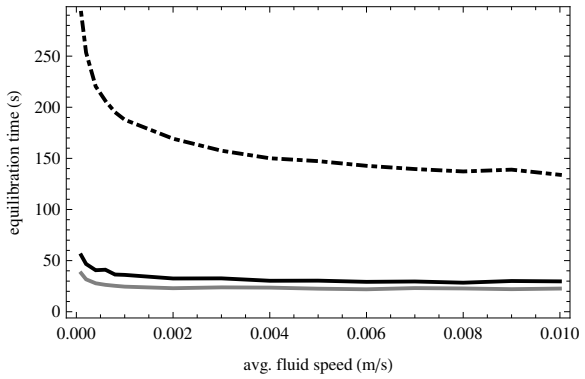

Fig. 4. Time to reach 90% of equilibrium binding as a function of average fluid speed v_{avg}. The curves are for different binding site densities, ρ_{binding}, of 5×10^{14}, 5×10^{15} and $5 \times 10^{16}/\text{m}^2$, from bottom to top, respectively. These all used the same temperature $T = 37°\text{C}$.

are needed for different binding site densities that are known before hand.

IV. Microarray Hybridization Automation

Automation is important for high throughput and reliability of a physical or chemical process, especially when multiple factors may contribute to the final output. The first step to automate a process is to have a dynamic model that can be used for controlling effects of different physical parameters. Microarray hybridization is a good candidate for process automation. As discussed earlier, some efforts have been made in this regard, but the process is still not precisely controlled due to lack of a proper mathematical model.

The above dynamic model can be used for this purpose. The model can be converted to a control model and applied with available control approaches [18]. The goal is to control the temperature, velocity and substrate binding site density

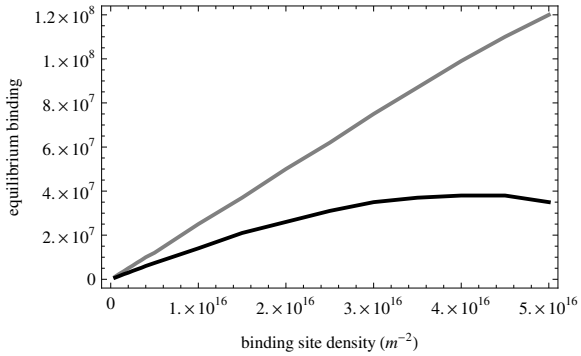

Fig. 5. Number of bound strands in equilibrium as a function of ρ_{binding}. The equilibrium values are independent of fluid speed. The two curves are for $T = 37°\text{C}$ and $T = 70°\text{C}$ for top and bottom, respectively.

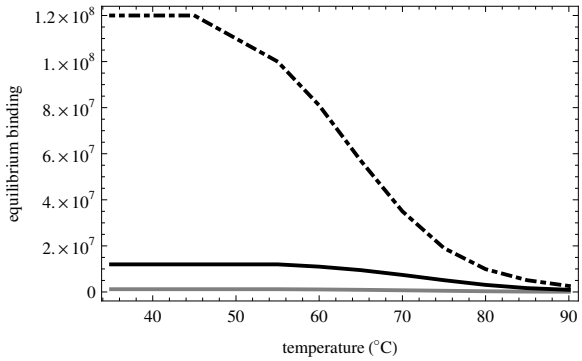

Fig. 6. Number of bound strands in equilibrium as a function of temperature. The equilibrium values are independent of fluid speed. The three curves are for different binding site densities, ρ_{binding}, of 5×10^{14}, 5×10^{15} and $5 \times 10^{16}/\text{m}^2$, from bottom to top, respectively.

in the automated system to improve the hybridization efficiency. For example, for various binding sites, hybridization efficiency may be obtained by controlling hybridization temperature and fluid velocity. Similarly, for microarrays from different fabrication platforms, the hybridization efficiency can be made same by controlling the hybridization temperature and fluid velocity. More importantly, the automated system can control hybridization for large batches of microarrays; so that comparisons of the results among them can be made more precisely. Automation to adjust for these variables could reduce concerns from differences due to hybridization conditions. This would be a significant advantage for microarray analysis. Differing from automated systems in the market, the proposed system is expected to have precisely and optimally control outputs on hybridization dynamics for various DNA microarrays.

V. Conclusions

This paper has proposed a dynamic model of DNA hybridization at the microarray surface in moving fluid. The model can be used to understand hybridization dynamics and how microarray hybridization results may be affected by fluidic dynamics and environmental factors. The goal of this model is to control the hybridization dynamics and automate

the microarray hybridization process; so that the microarray can generate higher fluorescence intensities in shorter periods of time.

Simulations were conducted and compared with results in the literature. In addition to overall performance, measured by hybridization efficiency, the model also shows more local features of the binding. For example, the spatial pattern of binding is not uniform. Instead, the behavior of diffusion related reactions has most activity at the edges of reactive patch, both upstream and downstream edges, in contrast to what might be expected from deterministic flow with binding progressing mainly from the upstream to downstream ends.

One application for the model presented here is for control, i.e., selecting parameters to optimize binding efficiency. Another application is feedback control for lab-on-a-chip hybridization, in which temperature, sample concentration and channel properties depend strongly on the hybridization environment. A precise feedback hybridization control system can ensure the maximum efficiency and signals by responding to changing environments with proper hybridization temperature or concentration to obtain the best signals. This is critical for many lab-on-a-chip applications, in which the signal to noise ratio is often quite sensitive to these external factors.

REFERENCES

[1] E. F. Petricoin III et al. Medical applications of microarray technologies: a regulatory science perspective. *Nature Genetics*, 32:474–479, 2002.

[2] F. J. T. Staal et al. DNA microarrays for comparison of gene expression profiles between diagnosis and relapse in precursor-B acute lymphoblastic leukemia: choice of technique and purification influence the identification of potential diagnostic markers. *Leukemia*, 17(7):1324–1332, 2003.

[3] A. E. Nkodo et al. Diffusion coefficient of DNA molecules during free solution electrophoresis. *Electrophoresis*, 22:2424–2432, 2001.

[4] Chii-Chang Chen et al. Enhancement of DNA hybridization efficiency using photovoltaic effect. In *Proc. of the 5th Pacific Rim Conference on Lasers and Electro-Optics*, volume 2, pages 733–739, 2003.

[5] Alexander W. Peterson, Richard J. Heaton, and Rosina M. Georgiadis. The effect of surface probe density on DNA hybridization. *Nucleic Acids Research*, 29:5163–5168, 2001.

[6] R. Bruce Wallace et al. Hybridization of synthetic oligodeoxyribonucleotides to $\phi\chi174$ DNA: the effect of single base pair mismatch. *Nucleic Acids Research*, 6(11):3543–3557, 1979.

[7] Alia H. Marafie. *Fast and Sensitive DNA Hybridization through Micro-Fluidics*. PhD thesis, Univ. of California, Irvine, 2005.

[8] J. Bishop, S. Blair, and A. M. Chagovetz. A competitive kinetic model of nucleic acid surface hybridization in the presence of point mutants. *Biophysical Journal*, 90:831–840, 2006.

[9] J. H. Kim et al. Characterization of DNA hybridization kinetics in a microfluidic flow channel. *Sensors and Actuators*, 113:281–289, 2006.

[10] Alexander L. Fetter and John Dirk Walecka. *Theoretical Mechanics of Particles and Continua*. McGraw-Hill, NY, 1980.

[11] Howard C. Berg. *Random Walks in Biology*. Princeton Univ. Press, 2nd edition, 1993.

[12] V. Chizhikov et al. Detection and genotyping of human group a rotaviruses by oligonucleotide microarray hybridization. *J. Clin Microbiol.*, 40(7):2398–2407, 2002.

[13] G. A. Held, G. Grinstein, and Y. Tu. Modeling of DNA microarray data by using physical properties of hybridization. *Proc. of the Natl. Acad. of Sci.*, 100:7575–7580, 2003.

[14] Frank F. Bier, Frank Kleinjung, and Frieder W. Scheller. Real-time measurement of nucleic-acid hybridization using evanescent-wave sensors: steps towards the genosensor. *Sensors and Actuators B: Chemical*, 39(1-3):78–82, 1997.

[15] Masanori Gotoh, Yukio Hasegawa, Yasuro Shinohara, Mizuho Shimizu, and Mariko Tosu. A new approach to determine the effect of mismatches on kinetic parameters in DNA hybridization using an optical biosensor. *DNA Research*, 2(6):285–293, 1995.

[16] David Erickson, Dongqing Li, and Ulrich J. Krull. Modeling of DNA hybridization kinetics for spatially resolved biochips. *Analytical Biochemistry*, 317:186–200, 2003.

[17] O. Henegariu et al. Multiplex PCR: Critical parameters and step-by-step protocol. *Biotechniques*, 23:504–511, 1997.

[18] Mingjun Zhang, Bradley Nelson, and Robin A. Felder, editors. *Life Science Automation: Fundamentals and Applications*. Artech House Publishers, Boston, 2007.